

Dynamic Actin Controls Polarity Induction *de novo* in Protoplasts

Beatrix Zaban*, Jan Maisch and Peter Nick

Botanical Institute, Molecular Cell Biology, Karlsruhe Institute of Technology, Kaiserstr. 2, D-76128 Karlsruhe, Germany

* Corresponding author

Tel: +49 721 608 42143; Fax: +49 721 608 44193; E-mail: beatrix.zaban@kit.edu

Available online on 6 November 2012 www.jipb.net and www.wileyonlinelibrary.com/journal/jipb

doi: 10.1111/jipb.12001

Abstract

Cell polarity and axes are central for plant morphogenesis. To study how polarity and axes are induced *de novo*, we investigated protoplasts of tobacco *Nicotiana tabacum* cv. *BY-2* expressing fluorescently-tagged cytoskeletal markers. We standardized the system to such a degree that we were able to generate quantitative data on the temporal patterns of regeneration stages. The synthesis of a new cell wall marks the transition to the first stage of regeneration, and proceeds after a long preparatory phase within a few minutes. During this preparatory phase, the nucleus migrates actively, and cytoplasmic strands remodel vigorously. We probed this system for the effect of anti-cytoskeletal compounds, inducible bundling of actin, RGD-peptides, and temperature. Suppression of actin dynamics at an early stage leads to aberrant tripolar cells, whereas suppression of microtubule dynamics produces aberrant sausage-like cells with asymmetric cell walls. We integrated these data into a model, where the microtubular cytoskeleton conveys positional information between the nucleus and the membrane controlling the release or activation of components required for cell wall synthesis. Cell wall formation is followed by the induction of a new cell pole requiring dynamic actin filaments, and the new cell axis is manifested as elongation growth perpendicular to the orientation of the aligned cortical microtubules.

Keywords: Actin; axis formation; microtubules; polarity induction; tobacco BY-2 protoplasts.

Zaban B, Maisch J, Nick P (2013) Dynamic actin controls polarity induction *de novo* in protoplasts. *J. Integr. Plant Biol.* 55(2), 142–159.

Introduction

Multicellularity allows the assignment of different functions to individual cells. Cell differentiation implies that individual cells have to upregulate specific functions, balanced by the downregulation of other functions. The reduced functions must be compensated by neighbouring cells, culminating in a situation where individual cells cannot survive isolated from the organismic context (Lintilhac 1999). The primordial form of cell differentiation is developmental dichotomy, which is characteristic of the first formative cell division of zygotes or spores in many algae, mosses and ferns, and the first division of the angiosperm zygote. Developmental dichotomy stems from a gradient of developmental determinants within the progenitor

cell that are then differentially partitioned to the daughter cells (formative cell division). Since the eighteenth century, the development of such gradients along an originally more-or-less homogeneous axis has been termed “polarity”. This concept simply designates the specific orientation of activity in space, and involves no assumptions whatsoever as to its causes (Bloch 1965).

How cells acquire polarity and axes remains a central question of development. Whereas polarity in animals is usually systemic in nature and is generated through the interaction of different cell types, plant polarity seems to be rooted directly in the individual cell. Although polarity of individual cells can be adjusted in a flexible manner, the global polarization of an organ represents the integration of these

individual polarities and therefore is relatively stable (Vöchting 1878).

Cell polarity in higher plants has been associated with the directional flux of the plant hormone auxin linked with the polar distribution of auxin-efflux carriers such as the PIN proteins (for recent review, see Peera et al. 2011). Efflux carriers are dynamically recycled between their active site at the plasma membrane and intracellular stores. This recycling differs between the different flanks of the cell, establishing a polar distribution (Dhonukshe et al. 2008). Interference with this recycling, for instance, by manipulation of the Rab5 GTPase pathway, can cause aberrant distributions of auxin and even redetermination of organs resembling homeotic mutations. Direction-dependent recycling as a mechanism to build polarity relies on a dynamic directional lattice. This lattice seems to be the actin cytoskeleton (Nick 2010).

The cell axis is a prerequisite for polarity, but is laid down by independent mechanisms in higher plants. Here, it is not actin, but cortical microtubules that define the biophysical properties of the yielding cell wall and thus the geometry of expansion. The classical model assumes that cortical microtubules define the orientation in which newly-synthesized cellulose microfibrils are laid down (reviewed in Geitmann and Ortega 2009; Nick 2011). In fact, fluorescently-tagged cellulose synthases have been shown to move in tracks adjacent to the subtending cortical microtubules (Paredes et al. 2006), and a protein interacting with cellulose synthase (CS11) has been shown to bind microtubules directly (Li et al. 2012). In cylindrical cells, where isotropic action of turgor pressure is predicted to produce only half of the strain in the longitudinal direction relative to the transverse direction, a transverse orientation of cellulose microfibrils maintains the lateral reinforcement needed to drive elongation (Green 1980). Based on situations where a transverse cellulose orientation persisted even though microtubules had been eliminated by drug treatment or temperature-sensitive mutations, a self-organization of cellulose has been proposed. During cell elongation, microtubules would sustain cellulosic self-organization by constraining the secretion of non-cellulosic polysaccharides (Fujita et al. 2011). Irrespective of the underlying mechanisms (that are not mutually-exclusive), the cell axis is linked to microtubules rather than actin filaments.

The orientation of cortical microtubules defines the orientation of division-related microtubule structures (preprophase band, spindle apparatus). In contrast to microtubules, the organization of actin filaments mostly persists during cell division. Therefore, the axis and polarity of the daughter cells are mostly inherited from the maternal cell (Nick 2011), raising the question of how polarity and axis are established *de novo*. To address this question, systems are required where polarity is induced outside of a tissue context.

A classical system for polarity induction is the *Fucus* L. zygote (Goodner and Quatrano 1993; Hable and Hart 2010). This

spherical cell divides asymmetrically, giving rise to a rhizoid and a thallus progenitor cell. This formative cell division can be oriented by unilateral blue light, whereby the rhizoid will form at the shaded flank. Much earlier than any morphological changes, a calcium flux is observed that progressively increases in amplitude by redistribution of influx towards the prospective rhizoid pole, and a concomitant efflux at the prospective thalloid pole (Jaffe 1966). Subsequently, a cap of fine actin filaments is observed at the rhizoid pole, attracting a pronounced flow of vesicles carrying cell wall material which causes a bulge as the first manifestation of the incipient rhizoid. The observation that, under strong plane-polarized blue light, a high fraction of birhizoidal twins can be induced, clearly demonstrates a true *de novo* generation of polarity. Although this beautiful system has been a classical object of physiological and cell biological studies of polarity formation, it suffers from limited molecular accessibility.

In higher plants, spherical cells that undergo formative divisions are rare. Even developing pollen shows a clear preformed directionality that during gametophytic development becomes manifest as directional movements of the nucleus and the organelles, and as asymmetric cell fate of the daughter cells (immortal generative cells, and mortal vegetative cell). This innate directionality seems to be linked with the cytoskeleton, because the assignment of different cell fates to the daughter cells can be equalized by anti-microtubular drugs (Twell et al. 1998).

As an alternative to studying polarity induction *de novo*, a loss of polarity can be caused artificially by digesting the cell wall with cellulases. This *tabula-rasa* approach yields protoplasts that, in most cases, are round and apparently have lost axes and polarity. Nevertheless, they can be induced to regenerate complete plants as demonstrated for the first time for tobacco (Nagata and Takebe 1970). Thus, protoplasts can generate axes and polarity *de novo*. They resemble *Fucus* L. zygotes in this respect. However, even a round protoplast can still maintain innate directionality. This became evident in a spectacular experiment, where entire maize (*Zea mays*) plants were regenerated after *in vitro* fertilization of a protoplasted egg cell by an isolated sperm cell (Lörz and Kranz 1993). Regeneration in this system was only successful when the sperm cell was fused in a specific site of the oocyte adjacent to the nucleus, indicating that the preformed polarity of the egg cell had persisted during cell isolation.

Despite this caveat, initial symmetry can be observed in regenerating protoplasts, providing an alternative to the *Fucus* L. system. In regenerating protoplasts of the moss *Physcomitrella patens*, it was possible to follow how calcium channels (visualized by a fluorescent channel antagonist) redistributed during regeneration and were assigned asymmetrically to one daughter cell, giving rise to the protonema (Bhatla et al. 2002). By the addition of auxin from an external source, the inhibition

of auxin efflux, and the inhibition of channel activity, both the polar redistribution of these channels as well as formative cell division can be blocked.

As illustrated by the example from mosses, a *tabula rasa* strategy using regenerating protoplasts would allow one to investigate polarity induction *de novo* without the constraints of the *Fucus* zygotes in systems that are more readily accessible to genetic engineering. Tobacco BY-2 cells have been widely used as a classical system for plant cell biology, mainly because mitosis can be readily synchronized, allowing biochemical approaches to the cell cycle (Nagata et al. 1992). However, this cell line is more than a mere plant version of the famous 'HeLa' culture, because the pluricellular files produced after subcultivation behave as a very simple organism with a clearly visible axis and polarity of the cell file, and a temporal pattern of individual cell divisions that are synchronized by a directional flow of auxin through the cell file (Maisch and Nick 2007; review in Nick 2010). Protoplasts of this cell line therefore represent a beautiful system to study the generation of axes and polarity *de novo*. In addition, fluorescently-tagged marker lines can be easily generated in this model, which allows for live cell imaging of the morphogenetic process. Since the cytoskeleton seems to control axis and polarity of plant cells, the cytoskeleton is expected to undergo dynamic remodeling during protoplast regeneration. In fact, microtubules can be aligned by mechanic force in regenerating BY-2 protoplasts, followed by an alignment cell elongation and division (Wymer et al. 1996), and F-actin is the most dynamic in isotropically expanding cells, with the density of actin filaments changing every 60 s (Smertenko et al. 2010).

In this study, we therefore followed bulk remodeling of the cytoskeleton in regenerating protoplasts of BY-2 using cells expressing fluorescently-tagged cytoskeletal markers. Upon standardization of the system, we were able to generate quantitative data on the temporal patterns of regeneration and the effect of anti-cytoskeletal compounds, inducible bundling of actin, RGD-peptides, and temperature. The occurrence of specific aberrations from the standard process allowed us to define the sensitive stages of the process, and lead to the conclusion that dynamic actin is required for axis induction, whereas microtubules are required for axis manifestation.

Results

Staging of protoplast regeneration

Using a protocol modified from Wymer and Cyr (1992), protoplast regeneration could be observed with a high degree of developmental homogeneity, which allowed us to define distinct stages of regeneration (Figure 1). Based on obvious or readily-detectable differences in cell shape and cell-wall

reformation, the vast majority of cells could be clearly assigned to one of four stages schematically represented in Figure 1A. Stage 0, prevailing at the end of digestion defined as $t = 0$, was comprised of round, completely symmetrical protoplasts lacking any indications for axis or polarity (Figure 1B, day 0). About 12–24 h later, a new cell wall is first synthesized, which is accompanied by vivid cytoplasmic streaming. The presence of a cell wall as visualized by staining with Calcofluor White defines stage 1. Although these cells still show radial symmetry, they already slightly deviate from a spherical shape expressed as local flattening (Figure 1B, day 1). Between day 1 and day 2 of regeneration, cell shape changes distinctly, and a clear cell axis emerges leading to an ovoid shape. This cell axis represents the criterion for stage 2 (Figure 1B, day 2). Subsequently, this axis becomes manifest as anisotropic expansion leading to cells, where the long axis is more than twice as long as the short axis, marking stage 3 (Figure 1B, day 3). At this stage, some of the cells begin to divide axially, producing the pluricellular files characteristic of tobacco suspension cells. These files are indistinguishable from those derived from walled cells. This general pattern of regeneration was observed in around 80% of the cells. However, a small but significant fraction of cells (around 20%) deviated from this canonical sequence, which will be described in more detail below.

The stages of protoplast regeneration are described in the following sub-paragraphs in detail. To get insight into the cellular mechanisms that drive regeneration and axis formation, the organization of microtubules and actin filaments was followed in protoplasts derived from cells expressing GFP-tagged markers for microtubules and actin filaments (Figure 2).

Stage 0: Upon staining with Calcofluor White, no fluorescence could be detected, indicating that cellulose is completely absent (Figure 2A). With differential interference contrast, the nucleus is seen to be positioned in the cell center, tethered to distinct transvacuolar cytoplasmic strands. Microtubules have lost their alignment in most protoplasts and are found in a random network in the cortex close to the membrane. However, in some cells, where microtubules appear to be slightly more bundled, alignment persists digestion of the cell wall (Figure 2B). Actin filaments are also randomly oriented in the cell cortex. The cortical network is connected by transvacuolar actin cables with the nucleus, which is encased by a perinuclear actin network (Figure 2C).

Stage 1: By staining with Calcofluor White, the reformation of cellulose can be used as a diagnostic marker for this stage (Figure 2D–E). As visible in the differential interference contrast (Figure 2D) in most (but not all) cells, the nucleus begins to shift from the cell center towards one of the lateral walls. As visible from confocal sections collected from the cortex (Figure 2E), the cellulose is not deposited homogeneously, but either in a meshwork (Figure 2D) or in thick fibers that often follow the direction of the underlying microtubular array,

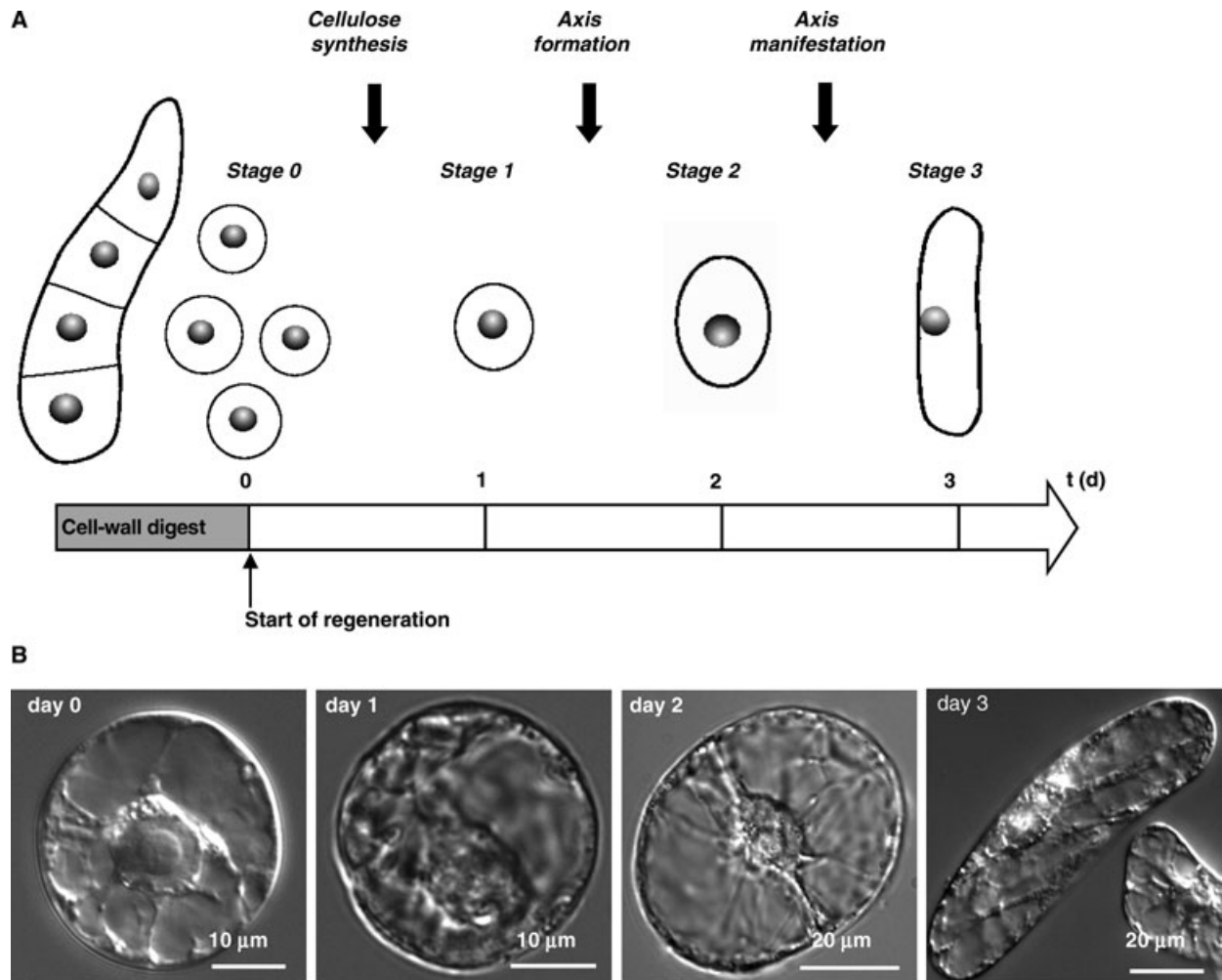


Figure 1. Regeneration of tobacco BY-2 protoplasts.

(A) Experimental design and definition of the stages used in the current study. Suspension cultures of tobacco BY-2 are digested by treatment with cellulase YC and pectolyase Y-23, washed to remove the enzymes, and transferred at $t = 0$, into regeneration medium containing synthetic auxin (NAA) and cytokinin (BAP). Regeneration can be subdivided into four distinct stages. *Stage 0* is defined by radial symmetry and the absence of cellulose, *stage 1* is defined by radial symmetry, but the presence of cellulose, *stage 2* is defined by a break of radial symmetry, *stage 3* is defined by the manifestation of cell axis.

(B) Representative differential-interference contrast images of BY-2 cells recorded at different time points of regeneration.

although they cannot be attributed to individual microtubules (Figure 2E). Microtubules, although showing local alignment, still do not reveal a clear global orientation. Often, microtubules of different orientations are crossed (Figure 2E) differently. A cortical network of fine actin filaments still does not reveal any preferential orientation (Figure 2F), whereby some filaments appear more distinct and thicker than others.

Stage 2: In these cells, a clear axis is laid down with the nucleus positioned closer to one “basal” cell pole (Figure 2G). The cellulose is now organized in parallel fibrils that cover the complete surface of the cell and are mostly aligned in a direction perpendicular with the long axis of

the cell. However, this alignment is not detected in the cell poles. The cortical microtubules are still randomly organized, but begin to align in a transverse direction. This alignment initiates in the region around the nucleus (Figure 2H), but, similar to cellulose microfibrils, it is not observed in the cell poles. Cortical actin filaments are now prominent, and distinct attachment sites at the cell periphery can be observed (Figure 2I). The perinuclear actin cage is now very distinct and brightly labelled.

Stage 3: The cells have undergone expansion in the long axis. Cellulose microfibrils are now clearly aligned in bundles perpendicular to this elongation axis (Figure 2J), the nucleus

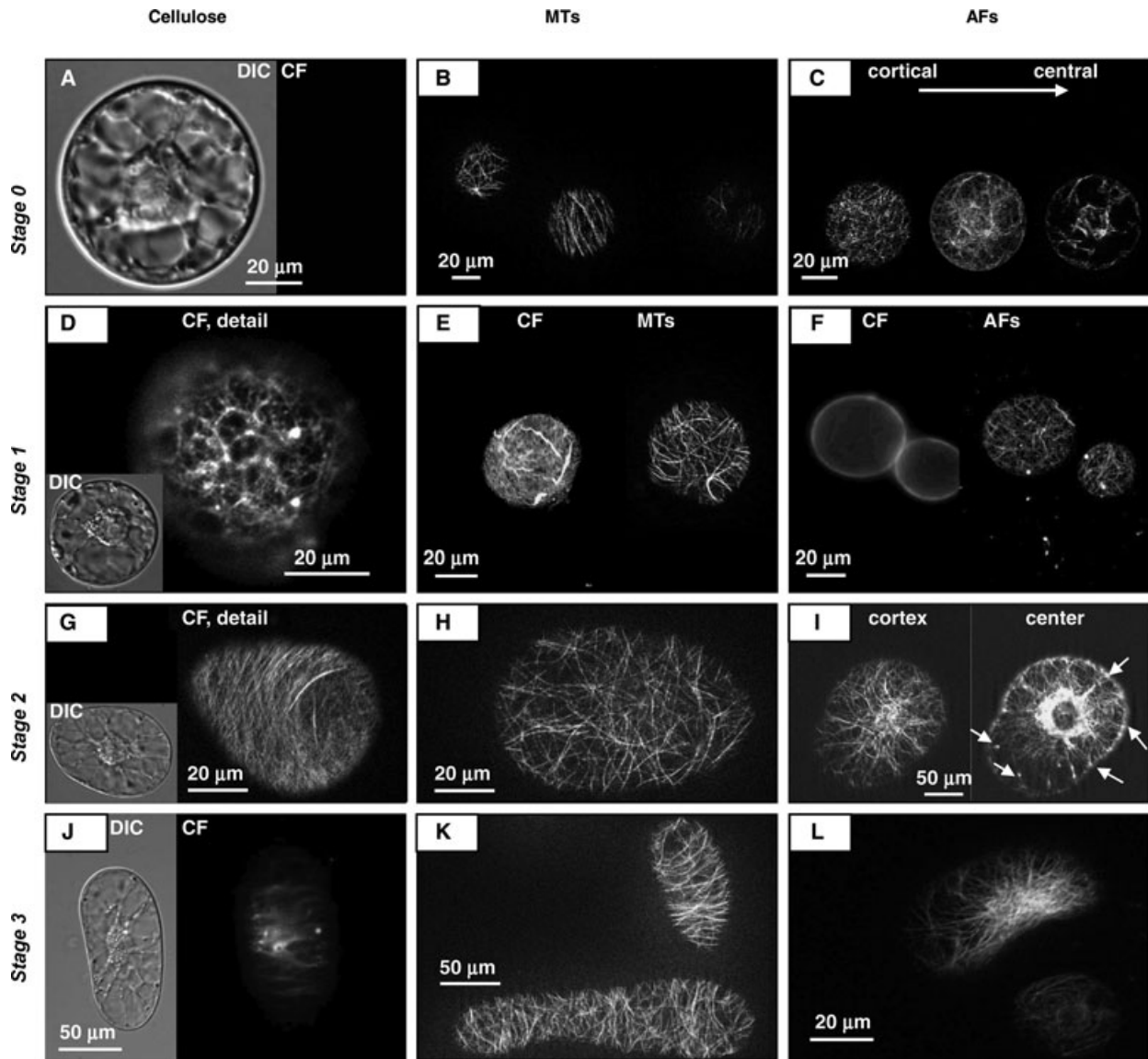


Figure 2. Cellular details of protoplast regeneration for the stages defined in Figure 1.

(A–C) *Stage 0*, (D–F) *stage 1*, (G–I) *stage 2*, (J–L) *stage 3*. (A), (D), (G), and (J) show cell morphology (differential interference contrast, DIC), and cellulose (Calcofluor White, CF). (B), (E), (H), and (K) show microtubules (MTs, GFP-AtTuB6), and (C), (F), (I), and (L) show actin filaments (AFs, GFP-FABD2). White arrows in (I) indicate adhesion sites for actin cables at the cell membrane.

is tethered to transvacuolar strands and has become elliptic, whereby its longer axis is parallel to the elongation axis. Cortical microtubules have increased in density, and are clearly aligned in parallel bundles perpendicular to the elongation axis (Figure 2K). Compared to *stage 2*, the cortical network has become finer and less dense, whereas the network around the nucleus is dense and is linked by numerous transvacuolar strands with the cell cortex (Figure 2L).

The transition between *stages 0* and *1* was studied in more detail on the base of time-lapse series (Figure 3). This

transition is very dynamic and involves vivid reorganization of cytoplasmic architecture, including a rotation and repositioning of the nucleus (Figure 3A) culminating in a progressively lateral position. The resynthesis of the cellulosic wall is a rapid process that proceeds within a few minutes (Figure 3B), but occurs almost exclusively in cells where the nucleus has acquired a lateral position. The exact timing of this event differs between individual protoplasts, but the majority of cells go through this transition during the first 12–24 h after protoplasting.

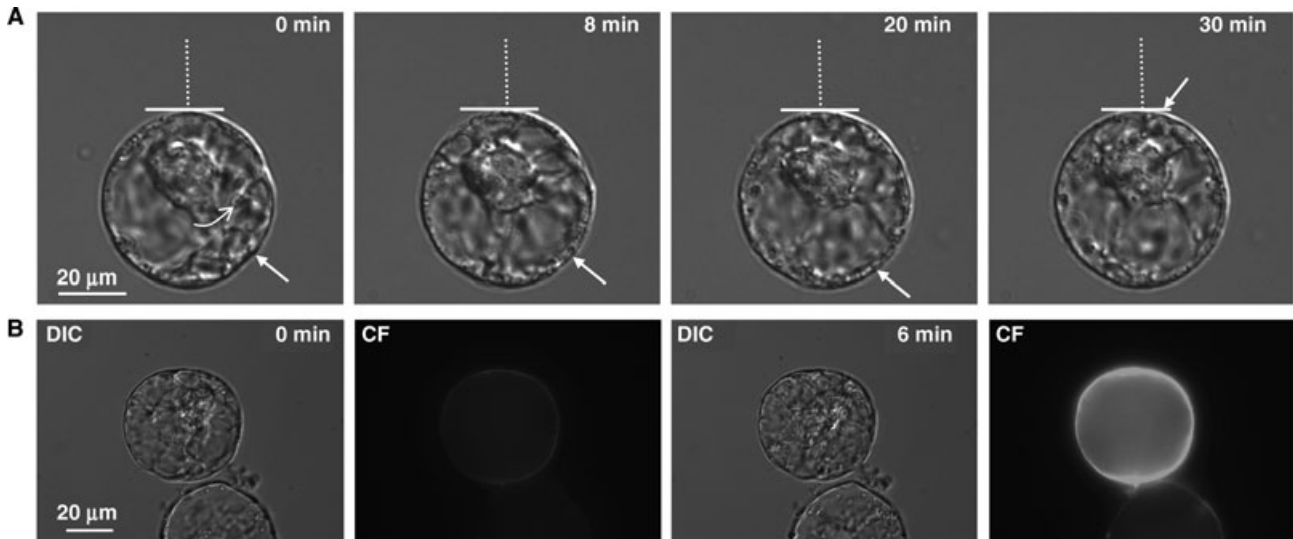


Figure 3. Time-lapse series of the transition from stage 0 to stage 1.

(A) Time series of nuclear movements in a protoplast during *stage 0*. Strong cytoplasmic streaming converges towards the sites indicated by arrows. The bent arrow indicates the direction of rotational movement, and the white line shows the position of the nuclear diameter with respect to the symmetry axis of the protoplast (dotted line).

(B) Time series of a protoplast at the transition from *stage 0* to *stage 1*. Note the strong increase in the Calcofluor White signal (CF) within a time interval of only 6 min.

Time course of protoplast regeneration

We were able to control the regeneration process to such a degree that a quantitative treatment became feasible. To validate the results from staging, we compared different non-transformed BY-2 cell lines at different time points originating from different labs, and obtained virtually the same frequencies for the different stages (**Figure S1**). The relative frequency of the stages was then charted over time (**Figure 4**). In addition to the non-transformed BY-2 cell line (**Figure 4A**), the tubulin marker line AtTuB6 (**Figure 4B**) and the actin marker line FABD2 (**Figure 4C**) were analyzed. The overall pattern was similar, with some specific differences for the marker lines that are described below.

After the first day of regeneration, the majority of protoplasts had left *stage 0* and reached *stage 1* or had even developed further to *stage 2* (**Figure 4A**). At day 2 of regeneration, cells in *stage 2* were predominant, whereas *stage 0* had decreased to a residual 5%, and *stage 1* had decreased to 30%. At day 3, more than 20% had reached *stage 3*, whereas *stage 2* had decreased to about 30% and *stage 1* had decreased to less than 20%. A fraction of cells diverged from the normal pattern of development. In some cells, the cell wall was laid down asymmetrically and was much thicker at the flank adjacent to the nucleus (**Figure 5A**), resulting in asymmetric elongation producing a sausage-shaped bending of the cell. In the remaining cells, a second competing axis was laid down, leading to a tripolar

situation whereby microtubules and cellulose fibers became aligned perpendicular to the adjacent cell pole (**Figure 5B**).

Regeneration of the AtTuB6 and the AtFABD2 lines shows specific deviations

Overall, the temporal pattern of regeneration in the AtTuB6 line (**Figure 4B**) was comparable to the situation in the non-transformed cell line. However, a closer look revealed that, in the AtTuB6 line, the early phases of regeneration were clearly promoted. After 1 d, more than 50% of the cells had advanced to *stage 2* (as compared to about 20% in the non-transformed cell line). The transition from *stage 2* to 3 was not promoted until day 3 (which means that the cells remained trapped in *stage 2*). However, during day 4, the fraction of the sausage-shaped cells with asymmetric elongation (**Figure 5A**) increased drastically compared to that observed in the non-transformed cell line.

Similar to the AtTuB6 line, the early phases of regeneration were promoted in the AtFABD2 line (**Figure 4C**). In addition, a significant proportion of cells did not produce a normal *stage 3* cell, but instead produced deviant sausage-shaped cells. The frequency of deviant tripolar cells increased, driving the fraction of deviant cells to roughly 60%.

To test whether the high frequency of tripolar cells in the AtFABD2 line might be linked to the slight stabilization

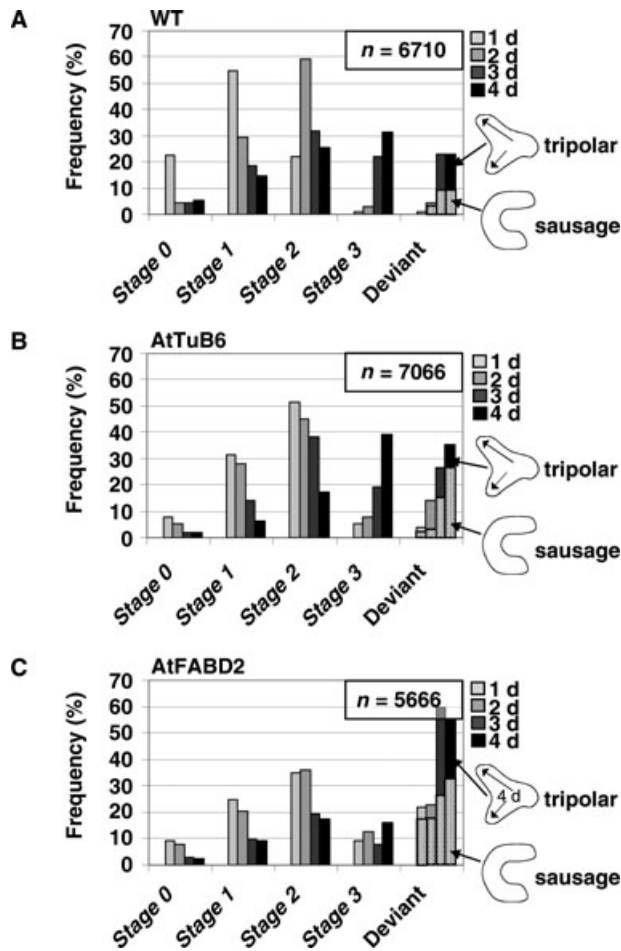


Figure 4. Time courses of regeneration stages.

The relative frequencies of each stage are shown for different time points in non-transformed BY-2 cells (wild-type, WT, **A**), cells expressing GFP in fusion with the microtubule marker AtTuB6 under control of the CaMV-35S promoter (AtTuB6, **B**), and cells expressing GFP in fusion with the actin marker AtFABD2 under control of the CaMV-35S promoter (AtFABD2, **C**). The frequency of cells deviating from the normal pattern is plotted as “deviant cells”. These included sausage-shaped cells and tripolar cells with branched polarity (details are given in **Figure 5**). The proportion of sausage-shaped cells is represented by the dotted bars. The frequency distributions have been calculated from 5,500 to 7,000 individual cells pooled from 30 independent experimental series.

of actin filaments reported for this marker (Holweg 2007; Wang et al. 2008), we tested a cell line where the actin-bundling LIM domain could be expressed under the control of a dexamethasone-inducible promoter (Thomas et al. 2007). When the inducer was added 1 d after the onset of regeneration, the pattern recorded at day 3 was the same as that in the non-induced control (**Figure 5B**). However, when the

inducer was added at the beginning, the frequency of deviant cells increased significantly (although it remained at around 35%, much lower than the 60% observed in the AtFABD2 line, compared with **Figure 4C**). This increase was due in equal parts to an increase of sausage-shaped and tripolar cells.

Effect of cytoskeletal drugs

Since both microtubules as well as actin filaments undergo a characteristic reorganization over the course of regeneration (**Figure 2**), and since expression of proteins binding to microtubules (AtTuB6, **Figure 4B**) and actin filaments (FABD2, **Figure 4C**; LIM-domain, **Figure 5B**) leads to specific morphogenetic aberrations, we tested the effect of cytoskeletal inhibitors (**Figure 6**).

Treatment of the non-transformed BY-2 line with 1 μ M of taxol, a microtubule stabilizer, clearly promoted the transition from *stage 0* to *stage 1* (**Figure 6A**). The frequency of *stage 2* was not significantly increased by taxol, but the frequency of sausage-shaped cells doubled compared to that observed in the control. Thus, the taxol treatment phenocopies several aspects observed in the AtTuB6 line (**Figure 4B**). A treatment with 0.5 μ M of taxol caused a similar response, but at a lower amplitude (data not shown).

A treatment of the non-transformed BY-2 line with 1 μ M of phalloidin, a stabilizer of actin, promoted the early transitions visible as a lower frequency of *stage 1* and a higher frequency of *stage 2* (**Figure 6D**). However, this was not followed by an increased frequency of *stage 3*. Instead, a much higher frequency of deviant cells was observed (from 14% in the control to 36% in the cells treated with 1 μ M phalloidin; treatment with 0.5 μ M phalloidin produced 32% deviant cells). Thus, the phalloidin treatment phenocopies the AtFABD2 line in several respects (**Figure 4C**).

The early phases of regeneration were promoted in the AtTuB6 line compared to the non-transformed control (**Figure 4B**). Since the integration of AtTuB6 might interfere with the dynamicity of microtubules by conferring a slight stabilization, we tested whether a wild-type pattern could be restored in the AtTuB6 line by a mild treatment with 1 μ M of Oryzalin (**Figure 6B**) that was sufficient to eliminate microtubules shifting the nucleus to one cell pole (**Figure 6E**). In fact, Oryzalin treatment slowed the transition from *phase 1* to *phase 2*, and consequently slowed the appearance of *stage 3* cells. Specifically, Oryzalin treatment restored the characteristic frequency peak of *stage 2* at day 2 of regeneration found in the non-transformed wild-type (compare the line “Ory” in **Figure 6B** with the line “control” in **Figure 6A**). Thus, a mild Oryzalin treatment can rescue a normal regeneration pattern in the AtTuB6 line.

In the AtFABD2 line, the early phases of regeneration were found to be promoted (**Figure 4C**). However, the later phases,

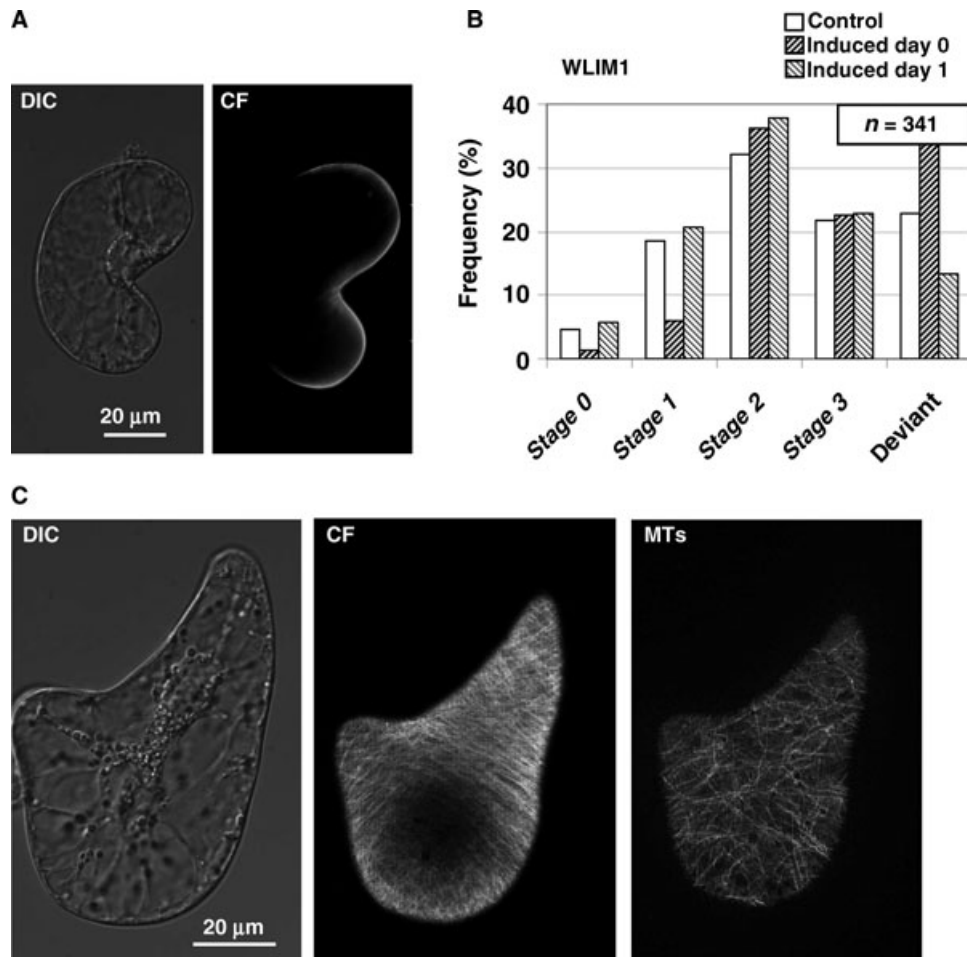


Figure 5. Details of deviant regeneration events.

(A) Sausage-shaped cell as frequently observed in the AtTuB6 line.

(B) Effect of dexamethasone-inducible actin bundling on the frequency of individual regeneration stages in the WLIM1 line scored at day 3. Dexamethasone was either added at time 0 or 1 day later. Note the decrease of normal *stage 1* and the increase of deviant cells for induction at time 0.

(C) Binuclear and bipolar cell at *stage 2* (day 2). DIC, differential interference contrast; CF, Calcofluor White signal; MTs, microtubules.

and most prominently the transition from *stage 2* to *stage 3*, were impaired, leading to a high frequency of deviant cells. Analogous to the Oryzalin experiment, we tested whether this line could be rescued by a mild treatment with 1 μ M of Latrunculin B with respect to the incidence of *stage 2* and *stage 3*. Latrunculin B sequesters G-actin monomers and thus eliminates actin filaments depending on their innate turnover. We observed that this treatment removed the cortical actin network and the transvacuolar strands that tether the nucleus to the cortex (Figure 6E). The perinuclear actin cage persisted, but the nucleus was again shifted to one cell pole similar to the situation after treatment with Oryzalin. The Latrunculin B treatment increased the frequency of *stage 2* cells (Figure 6D), and clearly rescued the incidence of *stage 3* to more than 30%,

which is the value that was observed in the non-transformed cell line (compare the line “Latrunculin B” in Figure 6D with the line “control” in Figure 6A). The incidence of deviant cells (around 60% observed at day 4 in the untreated AtFABD2 line) was reduced by about half to 32%. Thus, a mild treatment with Latrunculin B can rescue a normal regeneration pattern in the AtFABD2 line.

Temperature dependency of regeneration

The interaction with the cell wall renders the cytoskeleton resistant against cold (Akashi et al. 1990). If the interaction of the cytoskeleton with an extracellular matrix is driving individual steps of the regeneration, this should therefore become evident

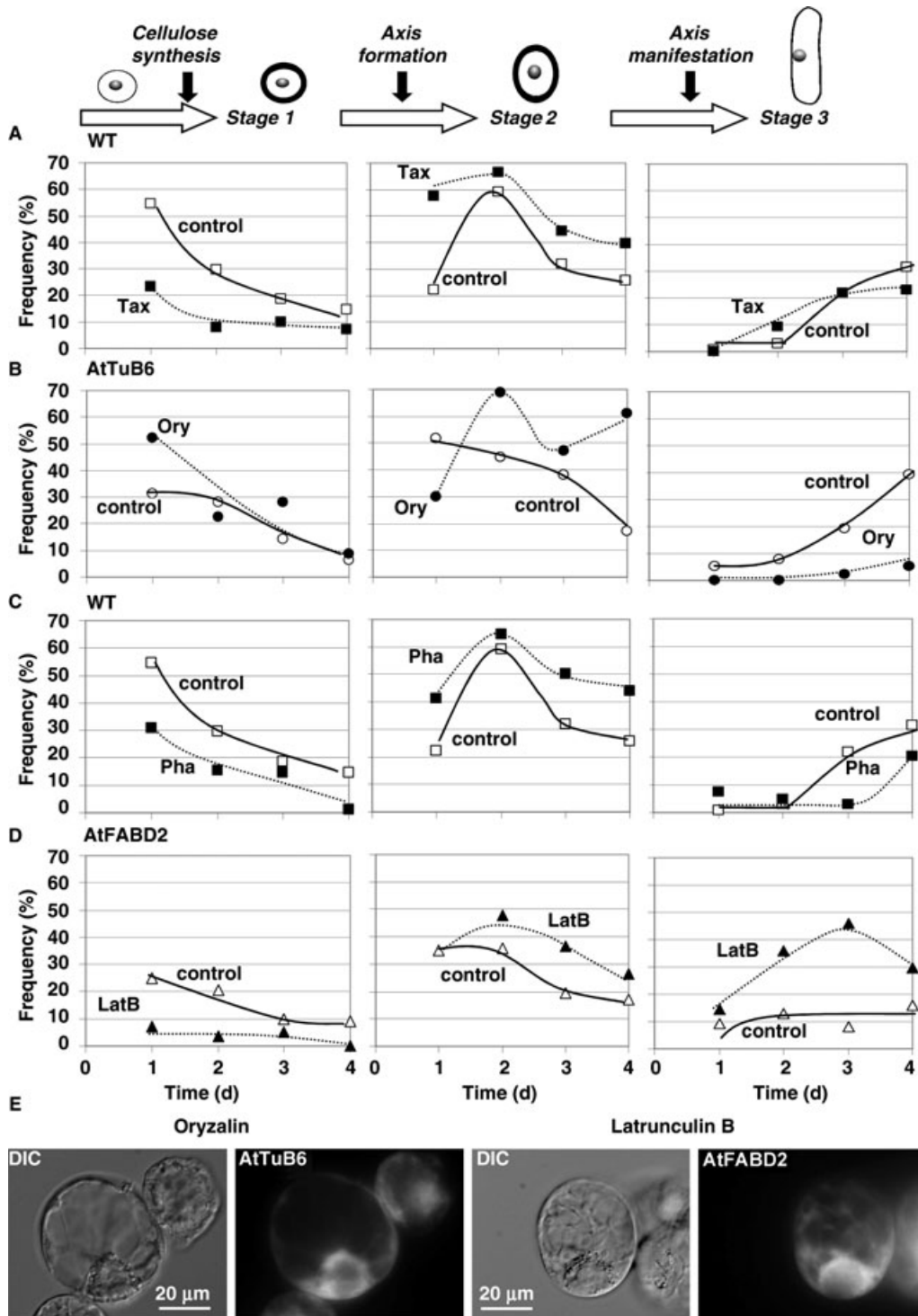


Figure 6. Effect of the cytoskeletal inhibitors on the temporal pattern of regeneration stages.

Stages 1 to 3 in non-transformed BY-2 cells (wild-type, WT, **A**, **C**), cells expressing GFP in fusion with the microtubule marker AtTuB6 under control of the CaMV-35S promoter (AtTuB6, **B**), and cells expressing GFP in fusion with the actin marker AtFABD2 under control of the CaMV-35S promoter (AtFABD2, **D**). Open symbols, non-treated cells; closed symbols, 1 μ M of taxol (**A**), Oryzalin (**B**), phalloidin (**C**) or Latrunculin B (**D**). The data represent populations of 500–1,000 individual cells. (**G**) Representative cells treated with 1 μ M Oryzalin (AtTuB6) or Latrunculin B (AtFABD2) at day 2. DIC, differential interference contrast.

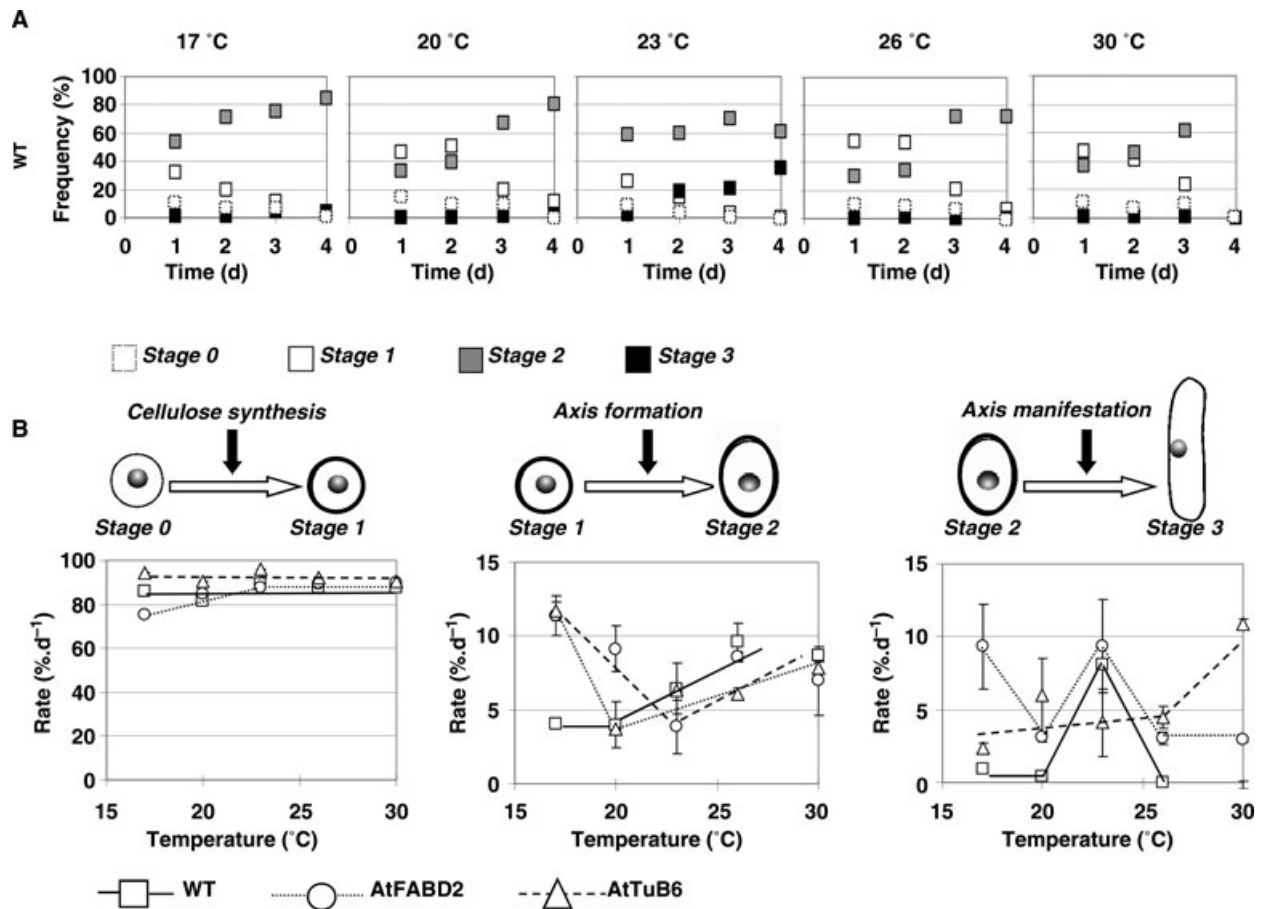


Figure 7. Effect of temperature on the temporal pattern of regeneration stages.

(A) Time course for the incidence of individual stages at different temperatures from 17 °C to 30 °C in non-transformed wild-type (WT) cells. **(B)** Temperature dependency for the rates of transition between the different stages in non-transformed BY-2 cells (WT), cells expressing GFP in fusion with the actin marker AtFABD2 under control of the CaMV-35S promoter (AtFABD2), and cells expressing GFP in fusion with the microtubule marker AtTuB6 under control of the CaMV-35S promoter (AtTuB6). Rates and standard errors were fitted based on a linear regression of relative frequencies over time (as shown for the WT in **A**) from populations ranging from 1,250 to 3,000 individual cells.

in the temperature dependency of the respective step. We therefore followed time courses of regeneration for different temperatures ranging from 17 °C to 30 °C, using intervals of 3 °C (non-transformed cells, **Figure 7A**; AtTuB6 and AtFABD2, **Figure S2**). This temperature was selected because it covers the physiological potency of BY-2 over which cells remain viable. From these time courses, transition rates (changes of frequency in % over time) could be deduced (**Figure 7B**). We observed that the transition from *stage 0* to *stage 1*, i.e. the regeneration of a cellulosic wall, was fairly independent of temperature in all three lines (**Figure 7B**, left graph). In contrast, the transition from *stage 1* to *stage 2*, i.e. the induction of a cell axis, was clearly dependent on temperature (**Figure 7B**, central graph). For the non-transformed cell line, it was slow at temperatures of up to 20 °C, but doubled when the temperature

was raised from 20 °C to 26 °C and remained high between 26 °C and 30 °C. For the AtTuB6 and the AtFABD2 lines, the transition rates were high at low temperatures, decreased to the level of non-transformed cells at temperatures of 20 °C to 23 °C, and increased again at higher temperatures similar to the non-transformed cell line. The transition from *stage 2* to *stage 3*, i.e. cell elongation, showed a pronounced temperature window for non-transformed cells (**Figure 7B**, right graph), and the AtFABD2 line exhibited a maximal rate at 23 °C and low rates for temperatures that were lower or higher. In contrast, the AtTuB6 line showed an almost temperature-invariant elongation between 17 °C to 26 °C, which increased steeply at 30 °C.

To gain further insight into these patterns, mortality was scored at the transition between *stage 1* and *stage 2*, and

the transition between *stage 2* and *stage 3*. For the non-transformed cell line, mortality was low for temperatures below 26 °C, but increased drastically at higher temperatures (Figure S3). The AtTuB6 line showed a parallel pattern with generally reduced mortalities at day 2. The AtFABD2 line contrasted with these results, exhibiting high mortalities at 17 °C and 20 °C for the transition from *stage 2* to *stage 3*.

These data suggest that the transition from *stage 0* to *stage 1*, i.e. the regeneration of a cellulosic wall, is mostly independent of temperature, whereas the subsequent transition from *stage 1* to *stage 2*, i.e. axis induction, requires a minimal temperature to proceed efficiently. Here, the expression of the AtTuB6 and the AtFABD2 marker accelerates axis induction at low temperatures. However, this acceleration effect disappears when the temperature is raised to 23 °C. The transition from *stage 2* to *stage 3*, i.e. axis manifestation as cell elongation, is sensitive to low and high temperatures, which in the case of the AtFABD2 line is accompanied by a high mortality rate at temperatures below 23 °C. In contrast, the expression of the AtTuB6 marker seems to stabilize cell elongation against fluctuations of temperature, which is also mirrored by reduced mortality.

RGD-peptides promote axis formation and manifestation

The heptapeptide YGRGDSP (termed “RGD”) mimics the adhesive motif of fibronectin and vitronectin recognized by animal integrins, and has been shown to interact with unknown plant components that mediate interactions of cytoplasmic strands with the extracellular matrix (Canut et al. 1998). Since axis formation (*stage 2*) is preceded by deposition of a new cellulosic wall (*stage 1*) which points to an interaction between the cytoskeleton and extracellular components (Wyatt and Carpita 1993), we asked whether it would be possible to titrate this putative interaction with RGD-peptides. As a control, we employed the heptapeptide YGDGRSP (termed “DGR”), which has been reported to be inactive (Canut et al. 1998). In non-transformed cells, treatment with 1 ng·ml⁻¹ of RGD peptides promoted the transition from *stage 1* to the subsequent *stages 2* and *3* (Figure 8A), leading to a reduced frequency of cells in *stage 1* and increased frequencies of cells in *stages 2* and *3*. Treatment with the same concentration of DGR peptides produced an intermediate behaviour: during the initial phase of the experiments (up to day 1), values were close to those observed in controls without peptides. From day 2 onward, the values obtained for treatment with DGR peptides approached those of treatment with the RGD peptides. Compared to RGD peptides, DGR was even more effective in enhancing the frequency of *stage 3* cells. In a preparatory study, we varied the concentration of peptides from 1 ng·ml⁻¹ to 10 ng·ml⁻¹, but failed to trigger a stronger effect, suggesting

that 1 ng·ml⁻¹ had already saturated the effect. We further observed that for concentrations exceeding 3 ng·ml⁻¹, the difference between RGD and DGR peptides merged progressively until (at 10 ng·ml⁻¹) the effect was identical independent of the peptide sequence, suggesting non-specific interactions. Protoplasts treated with RGD peptides tended to aggregate, flattening at the domains of contact. Neither untreated controls nor DGR-treated protoplasts showed this phenomenon (data not shown). When this study was extended to AtTuB6 (Figure 8B) or AtFABD2 (Figure 8C) cells, the same effect pattern as in the non-transformed cells was observed: the incidence of cells in *stage 1* decreased, whereas cells in *stages 2* and *3* became more frequent, and the DGR produced intermediate effects.

Discussion

Nuclear migration as a pacemaker for polarity induction?

The formation of a new cell wall (leading to *stage 1*) represents a crucial step in regeneration. With a duration of around 1 day, it limits the rate of the entire process. The newly-regenerated walls lack the directional texture characteristic of axially growing plant cells, and their synthesis is preceded by intensive dynamics of cytoplasmic architecture, including active migration of the nucleus. Interestingly, cell wall synthesis does not proceed gradually, but becomes manifest as a sudden, saltatory transition happening within a few minutes. The time point of this transition differs widely over the population of cells, and for a given cell it proceeds within a very short window of time.

We probed for the role of microtubules in this event, and observed that cell wall regeneration was promoted in the AtTuB6 marker line, which could be phenocopied in the non-transformed wild-type by treatment with the microtubule stabilizer taxol. Conversely, the promotion of cell wall formation in the AtTuB6 line could be reverted by treatment with Oryzalin, a compound that sequesters tubulin heterodimers and thus causes a destabilization of dynamic microtubules. Our data not only suggest that microtubule stability promotes the synthesis of a new cell wall, but also that the expression of the ectopic tubulin AtTuB6 confers a slight but significant stabilization to microtubules.

The situation for actin filaments is similar: cell wall regeneration is promoted in the AtFABD2 marker line, which was phenocopied in the non-transformed wild-type by treatment with the actin stabilizer phalloidin. Conversely, the promotion in the AtFABD2 line could be reverted by treatment with Latrunculin B, sequestering actin monomers and thus destabilizing dynamic actin filaments. Similar to microtubules, actin filament stability promotes the synthesis of a new cell wall. Again,

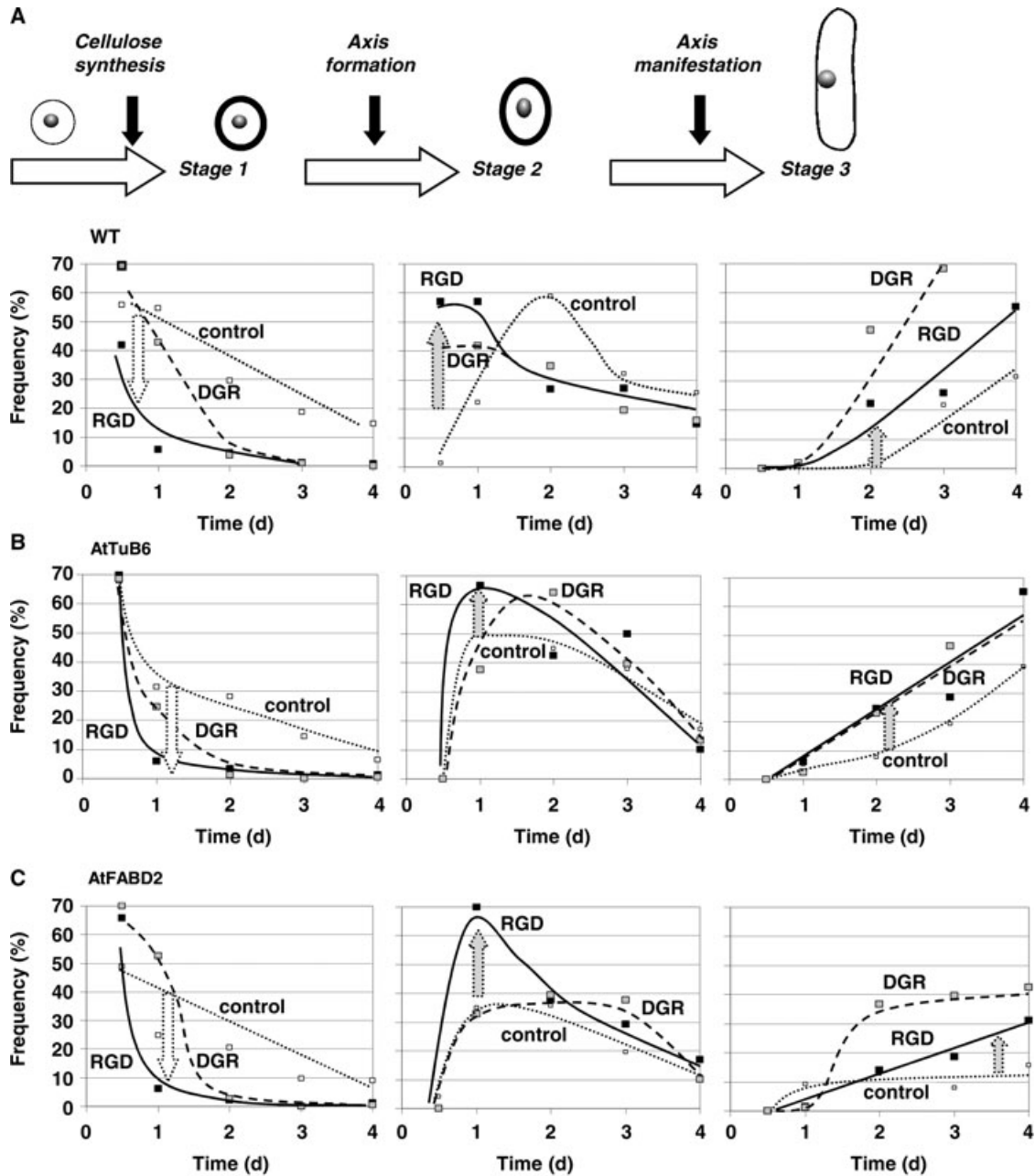


Figure 8. Effect of the heptapeptide YGRGDSP on the temporal pattern of regeneration stages.

Stages 1 to 3 in non-transformed BY-2 cells (wild-type, WT, **A**), cells expressing GFP in fusion with the microtubule marker AtTuB6 under control of the CaMV-35S promoter (AtTuB6, **B**), and cells expressing GFP in fusion with the actin marker AtFABD2 under control of the CaMV-35S promoter (AtFABD2, **C**). Open squares, non-treated cells; black squares, 1 ng mL^{-1} of the pentapeptide YGRGDSP; grey squares, 1 ng mL^{-1} of the pentapeptide YGDGRSP added at time 0. The data represent populations of 300–2,000 individual cells.

the expression of the fluorescent actin marker (FABD2, the actin-binding domain of plant fimbrin) confers a slight stabilization of actin filaments consistent with the published record for this probe (Holweg 2007; Wang et al. 2008). Since the cortical

actin array is extremely dynamic with filament lifetimes in the range of 30 s (Staiger et al. 2009), any function dependent on this actin array is expected to be extremely sensitive to actin stabilization.

At the transition from *stage 0* to *stage 1*, neither microtubules nor actin filaments show any significant alignment, which is mirrored by the absence of directional texture in the deposited cellulose. RGD peptides promote the transition to *stage 1*, and at the same time this transition is well buffered against changes in temperature. These observations can be incorporated into a working model for the cellular events driving induction of axis and polarity in the regenerating protoplast (Figure 9).

The enzyme complexes synthesizing cellulose are transported from the Golgi apparatus to the plasma membrane in exocytotic vesicles (Haigler and Brown 1986), but can only function upon integration of these vesicles into the plasma membrane. The sudden appearance of cellulose within a few minutes (Figure 3B) suggests that these vesicles are not continuously inserted into the membrane, but first accumulate beneath it and remain in place until they are released simultaneously. This is consistent with a previously proposed model (Emons and Mulder 1998), whereby cell wall synthesis is confined to so-called activation zones, where the constrained fusion of the exocytotic vesicles loaded with the cellulase synthetase is released by a signal (possibly a calcium wave). In the regenerating protoplast, this releasing signal correlates with the positioning of the nucleus that undergoes intensive movements prior to cell wall resynthesis (Figure 3A). Since both cellulose and vesicle transport require the addition of chemical energy, they should depend strongly on temperature. In this

background, the pronounced temperature compensation for the transition from *stage 0* to *stage 1* is unexpected at first sight. However, cellulose synthesis is not the rate-limiting process here, because it can proceed within a few minutes, once the vesicles containing the cellulose synthetases have fused with the plasma membrane. However, these vesicles have accumulated over a time span that seems to be sufficiently long to reach saturation, even for the lower temperatures leading to the observed (apparent) temperature compensation.

Why is the transition toward *stage 1* supported by cytoskeletal stability? The efficiency of exocytosis depends on the motility of the endoplasmic reticulum, which in turn is dependent on myosin activity and actin organization (Ueda et al. 2010). This dependency would explain why the transition to *stage 1* is promoted by the stabilization of actin and is delayed by its destabilization. It would also account for the effect of RGD peptides. RGD peptides can modulate cytoskeletal organization by interfering with the so-called cytoskeleton plasma membrane-cell wall continuum (for reviews see Baluška et al. 2003; Pickard 2007), and therefore are expected to modulate the transition to *stage 1* as well. The role of microtubule stability is less evident. The cellulase-interacting protein CSI has been shown to bind microtubules directly *in vitro* (Li et al. 2012), adding further molecular proof to the so-called microtubule-microfibril hypothesis proposed half a century ago (Green 1962). However, this hypothesis dealing with the oriented deposition of cellulose

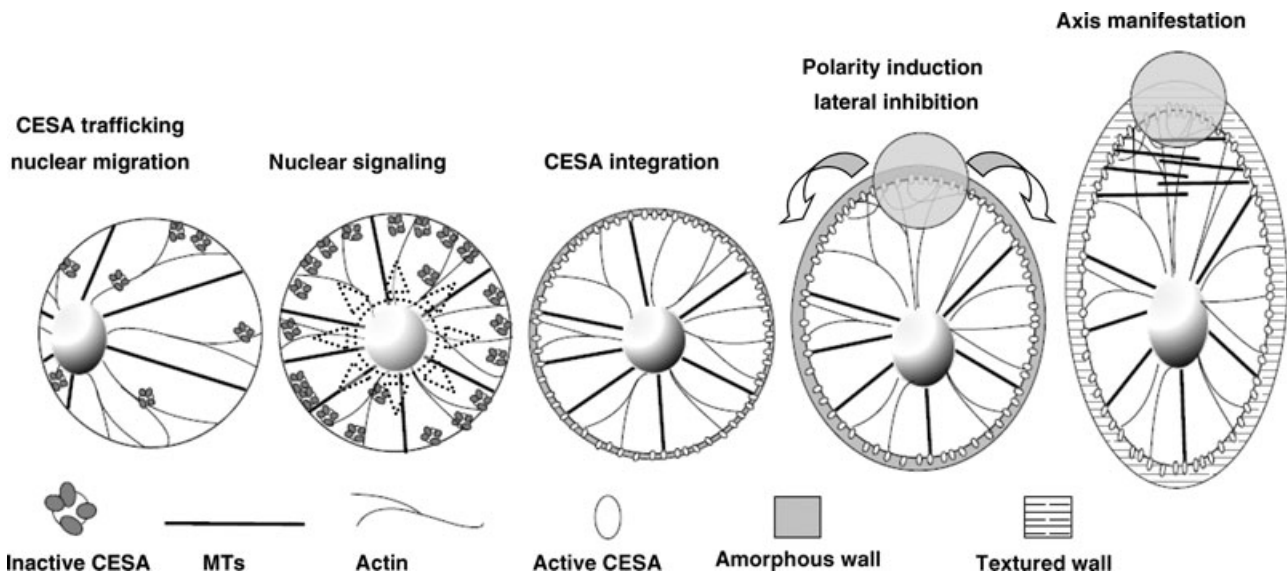


Figure 9. Working model for polarity induction in regenerating protoplasts.

During *stage 0*, vesicles containing cellulose-synthetases (CESA) are transported towards the membrane, but are not inserted. Simultaneously, the nucleus is repositioned by the cytoskeleton. When the nucleus has reached the cell center, a signal is released that will trigger integration of CESA into the membrane followed by rapid synthesis of amorphous cellulose. A cell pole is defined that will laterally inhibit the formation of ectopic competitors. This inhibition requires dynamic actin. Cortical microtubules align in a perpendicular orientation, reinforcing cell elongation.

microfibrils does not address why microtubules should stimulate the synthesis of cellulose per se (although the microtubule-microfibril hypothesis is relevant for the subsequent stages of regeneration as will be discussed below). It is a second function of microtubules that has to be considered in this context: microtubules, through unconventional, plant-specific, minus-end-directed KCH kinesins (Klotz and Nick 2012), control the positioning and tethering of the nucleus preceding the appearance of a new cell wall. Nuclear positioning, in turn, has been found to act as pacemaker for mitosis (Frey et al. 2010), and is accompanied by extensive remodeling of cytoplasmic streaming (Figure 3A). This leads to the question of whether nuclear movements act as pacemakers for polarity induction. This mechanism seems to act in a classical case of polarity induction, the gravimorphosis of germinating fern protonemata: the direction of protonema outgrowth is determined by the gravity vector during a defined time window preceding germination, but cannot adjust its direction once it has germinated (Edwards and Roux 1994). During the time of gravity responsiveness, the nucleus of the spore undergoes vigorous movements that, as concluded from inhibitor studies, are driven by microtubules (Edwards and Roux 1997). In fact, the geometry of cell division is defined by microtubules emanating from the moving nucleus. These microtubules deposit a belt of endosomes that later, upon the completion of mitosis, are read out by a different set of “exploratory” microtubules (Dhonukshe et al. 2005). Our observations are consistent with the working hypothesis that the nucleus “explores” its position using microtubules. The nucleus might convey positional information through microtubules to the cell periphery and thus trigger the release of cellulase synthase-containing vesicles underneath the cell membrane (Figure 9).

Axis formation (polarity induction) requires dynamic actin

A small but not negligible fraction of cells deviated from the standard path of regeneration. Some of these cells were disturbed in axis manifestation leading to sausage-shaped bending, whereas in other cases, tripolar cells were generated. These deviations were markedly more frequent in the AtFABD2 line, where the lifetime of actin filaments is slightly, but significantly, increased (Holweg 2007; Wang et al. 2008). In fact, axis formation and manifestation could be perturbed by inducible expression of the actin-stabilizing LIM domain, and the high frequency of deviating cells in the AtFABD2 line (about 60%) could be reduced by application of Latrunculin B (to 32%) leading to a partial rescue of correct axis formation and manifestation. These findings lead to the conclusion that axis formation (and, consequently, axis manifestation) requires the extremely dynamic population of actin filaments subtending

the plasma membrane (Staiger et al. 2009). A conceptual base for this observation (Figure 9) might be the dynamic repartitioning of auxin-efflux carriers required to establish cell polarity (Dhonuskhe et al. 2008; for review see Peera et al. 2011), which in turn depends on dynamic actin (for review see Nick 2010). However, other actin-related processes such as anchoring of calcium channels or localized secretion proposed for zygote polarity in *Fucus* L. (Brawley and Robinson 1985) should be kept in mind. The promotion of stage 2 by RGD-peptides can be explained by the accelerated formation of a new cell wall discussed above, and suggests that the regeneration of a new cell wall is a prerequisite for polarity induction. We observed a pronounced temperature optimum for the transition to stage 2, which might arise from an antagonistic interaction between membrane fluidity and actin filaments, similar to the situation reported for cold acclimation (Örvar et al. 2000).

The tripolar cells resemble the structures observed in *Fucus* L., when the zygotes were irradiated with strong plane-polarized blue light (Jaffe 1966). These tripolar structures call for a critical discussion of terminology. Polarity can be expressed in two versions (Nick and Furuya 1992): as *complex polarity*, where both poles along an axis are explicitly defined by molecules or activities, or as *simple polarity*, where only one pole is defined explicitly, whereas the opposite pole is merely defined by the absence of the respective molecules or activities. The animal-vegetative polarity of sea-urchin eggs (Boveri 1901), the prestalk-prespore polarity of *Dictyostelium discoideum* (Williams 1988), or the head-foot polarity of *Hydra* (Bode and Bode 1984) provide classical examples for complex polarities. As pointed out more than a century ago by the plant physiologist Julius Sachs during a scientific debate with his opponent Vöchting (1878), any reorientation of complex polarities should result in a quadripolar situation (Sachs 1880). Tripolar situations as those observed here are indicative of perturbations of simple polarities, when a second, competing pole is ectopically laid down. In *Fucus* L., it is the site of prospective rhizoid outgrowth, which is explicitly defined by the accumulation of calcium influx channels and the actin cap, whereas the opposite thallus “pole” is not defined positively, but simply follows a default pathway proceeding in the absence of calcium influx and membrane-associated actin (Brawley and Robinson 1985; Goodner and Quatrano 1993). Irradiation with plane-polarized light will activate the (oriented and therefore dichroitic) photoreceptor to a similar extent in two sites of the zygote such that two competing rhizoid sites will develop, whereas the thalloid pole (which is actually just a “none-pole”) will remain undivided, leading to the observed tripolar structures. For complex polarities, a body axis appears concomitantly with or even prior to polarization. In contrast, simple polarities have to be established and read out as morphogenetic gradients before a body axis can be laid down. The tripolar structures

observed when actin dynamics are impaired during the initial phases of regeneration suggest that it is polarity induction rather than axis formation that drives the transition from *stage 1* to *stage 2*.

The symmetry of axis manifestation depends on microtubule dynamics

Following polarity induction / axis formation, cortical microtubules are progressively ordered into parallel arrays, accompanied by cell elongation in a direction perpendicular to microtubule orientation and a progressive alignment of cellulose texture with microtubules. The actin network is repartitioned in favor of perinuclear bundles that are interconnected with the cortical actin prevalent during the preceding stages. The AtTuB6 line, although promoted in the early transitions (up to *stage 2*), was trapped in *stage 2* and subsequently produced a high fraction of characteristic sausage-shaped aberrations. This phenotype could be partially phenocopied by taxol, and partially rescued by Oryzalin.

Axis manifestation (leading to *stage 3*) is based on elongation growth, which requires anisotropic cell expansion (Sijacic and Liu 2010). In expanding cylinders, mechanic tension is anisotropic (with transverse doubled over longitudinal tension), such that cylindrical plant cells are expected to widen rather than to elongate (Preston 1955). By transverse deposition of cellulose microfibrils, plant cells can override this mechanic anisotropy and reinforce elongation growth (Green 1980). Cortical microtubules can align cellulose orientation either by physical coupling with cellulose-synthase subunits through proteins such as CSI1 (Li et al. 2012), or by influencing cellulose self-organization through a control of cellulose crystallinity (Fujita et al. 2011). The setup of parallel microtubule arrays (transition from *stage 1* to *stage 2*) might be caused by disassembly of the randomly-oriented network found in *stages 0* and *1*, followed by a directional reassembly. Alternatively, microtubules might coalign by mutual sliding. Directional reassembly would be impaired when microtubules are stabilized by taxol or over-expression of the AtTuB6 marker. However, we observed that under these conditions, *stage 2* was advanced in time consistent with a model of mutual sliding. A promotion of microtubule alignment after treatment with taxol has also been reported by Kuss-Wymer and Cyr (1992). However, the readout of the cell axis from these microtubule arrays requires dynamic microtubules, since AtTuB6 cells are trapped in *stage 2* and exit with a high frequency into aberrant sausage-shaped aberrations. This aberration is accompanied by asymmetric deposition of the cell wall, very often linked with a strong asymmetry of nuclear positioning which is shifted towards the concave flank where the wall is thicker (Figure 5A). This phenotype indicates that microtubule dynamics are necessary to balance cell elongation at the two flanks of the elongating

cell. It is not straightforward to derive the observed thickness of the cell wall from altered orientation of cortical microtubules. However, the model already proposed for the transition from *stage 0* to *stage 1* might also account for the role of dynamic microtubules in axis manifestation (*stage 3*). A signal from the nucleus, conveyed through microtubules, might promote the integration of cellulose-synthase complexes into the membrane (Figure 9). The symmetry of this signal would be established depending on the dynamic instability of competing microtubule populations at the two flanks of the elongating cells. Through stabilizing microtubules, this geometrical cross-talk would be impaired such that cellulose synthesis at the cell wall adjacent to the nucleus would be uncoupled from the events at the opposite flank, resulting in the observed sausage phenotype. The promotion of axis manifestation by RGD peptides indicates a stabilizing function of the cytoskeleton plasma membrane-cell wall continuum consistent with the model of a regionally-differentiated membrane (Baluška et al. 2003; Pickard 2007). The feedback from the cell wall relies on dynamic actin filaments that are found to align with the elongation axis, consistent with the published record on elongating plant cells (Smertenko et al. 2010). It should be mentioned that, in this study, similar sausage-shaped aberrations were observed under conditions of sustained auxin depletion.

Outlook: probing the cytoskeleton-membrane interaction

Our analysis in regenerating protoplasts has identified microtubule-driven nuclear movements and cytoskeleton-membrane-cell-wall interaction as important factors for polarity and axis induction *de novo*. Microtubules as mechanically rigid structures can convey compression forces, whereas actin as flexible elements can convey traction forces. When both elements are linked by proteins such as the KCH-kinesins (Klotz and Nick 2012), a tensegral network emerges that can collect and integrate mechanic forces, which allows the cell to explore geometry (for review see Nick 2011). To test this concept, we will extend the experimental system worked out here towards mechanical interference. One approach will use nuclear displacement by mild centrifugation (Murata and Wada 1991). This strategy had already been successfully employed to align division axis with the force vector of centrifugation, and to demonstrate that microtubules are necessary and sufficient to sense the mechanical input (Wymer et al. 1996). We want to extend this approach towards assessing the role of microtubule-driven nuclear positioning on polarity induction. A second approach launched recently is based on microfluidics. Here, preformed geometries are enforced upon the regenerating protoplasts by providing rectangular vessels (Sun et al. 2009) that are oriented either in parallel or perpendicularly, with a flow of auxin as a polarizing chemical signal.

Materials and Methods

Cell lines and cultivation

BY-2 (*Nicotiana tabacum* L. cv Bright Yellow-2) suspension cell lines (Nagata et al. 1992) were cultivated in liquid medium containing 4.3 g/L Murashige and Skoog (MS) salts (Duchefa Biochemie), 30 g/L sucrose, 200 mg/L KH_2PO_4 , 100 mg/L (myo)-inositol, 1 mg/L thiamine, and 0.2 mg/L 2,4-D, pH 5.8. In addition to the non-transformed BY-2 wild-type (WT), transgenic lines were used in this study that expressed the actin-binding domain 2 of plant fimbrin in fusion with GFP under the control of the constitutive cauliflower mosaic virus (CaMV) 35S promoter (AtFABD2, Sano et al. 2005), the actin-bundling LIM-domain in fusion with GFP under the control of a glucocorticoid-inducible promoter (Thomas et al. 2007), or a transgenic line expressing the β -tubulin AtTuB6 from *Arabidopsis thaliana* in fusion with GFP driven by the CaMV 35S promoter (Hohenberger et al. 2011). The cells were subcultivated weekly, inoculating 1.0 to 1.5 mL of stationary cells into fresh medium (30 mL) in 100-mL Erlenmeyer flasks. The cells were incubated in darkness at 27 °C under constant shaking on a KS260 basic orbital shaker (IKA Labortechnik, Germany) at 150 rpm. The media for the transgenic cell lines were complemented with either 30 mg/L hygromycin (WLIM–GFP, AtFABD2) or with 50 mg/L kanamycin (AtTuB6–GFP), respectively.

Generation and regeneration of protoplasts

The protocol was adapted from Kuss-Wymer and Cyr (1992) with minor modifications. Aliquots of 3 mL were harvested under sterile conditions 3 d after subcultivation and digested for 6 h at 25 °C in 1% (w/v) cellulase YC (Yakuruto, Tokyo), and 0.1% (w/v) pectolyase Y-23 (Yakuruto, Tokyo) in 0.4 M mannitol at pH 5.5) under constant shaking on a KS260 basic orbital shaker (IKA Labortechnik) at 100 rpm in petri dishes of 90 mm diameter. For the non-transformed WT, 1.3 mL enzyme solution per mL of suspension were used, for AtFABD2 and WLIM 3 mL were used, and for AtTuB6 6 mL were used. After digestion, protoplasts were collected by 500 rpm for 5 min at 25 °C in fresh reaction tubes. The protoplast sediment was carefully resuspended in 10 mL of FMS wash medium (4.3 g/L MS-salts, 100 mg/L (myo)-inositol, 0.5 mg/L nicotinic acid, 0.5 mg/L pyroxidine-HCl, 0.1 mg/L thiamin and 10 g/L sucrose in 0.25 M mannitol; Kuss-Wymer and Cyr 1992; Wymer et al. 1996). After three washing steps, protoplasts were transferred into 1.5 mL FMS-store medium (FMS wash medium complemented with 0.1 mg/L 1-naphthaleneacetic acid (NAA), and 1 mg/L benzylaminopurin). Protoplasts were incubated in the dark at 26 °C without shaking in petri dishes (5 cm diameter), if not stated otherwise. To prevent evaporation, the petri dishes were sealed with parafilm. In some experiments, the FMS-store medium was complemented with 1 μM of Oryzalin (to eliminate

microtubules), taxol (to stabilize microtubules), Latrunculin B (to eliminate actin filaments), or phalloidin (to stabilize actin filaments). Alternatively, the pentapeptides YGRGDSP and YGDGRSP (Panatecs, Tübingen, Germany, purity > 75%) were added at 1–10 $\mu\text{g/L}$ to interfere with the extracellular matrix. Actin-bundling was induced in the WLIM line by addition of 100 $\mu\text{g/mL}$ of dexamethasone (Sigma-Aldrich, Neu-Ulm, Germany) to the FMS-store medium.

Microscopy and quantifications

15 μL of protoplast suspension were carefully mounted on slides using silicone-made imaging spacers (Secure-Seal, Sigma-Aldrich, Neu-Ulm, Germany) to avoid protoplast bursting. For staging (Figure 1), cellulose was stained by Calcofluor White (1 volume of 0.1% w/v) according to Maeda and Ishida (1967), and Nagata and Takebe (1970). Cells were examined under an AxioImager Z.1 microscope (Zeiss, Jena, Germany) equipped with an ApoTome microscope slider for optical sectioning and a cooled digital CCD camera (AxioCam MRm) recording the GFP signal through the filter set 38 HE (excitation at 470 nm, beamsplitter at 495 nm, and emission at 525 nm) and the Calcofluor White signal through the filter set 49 (excitation at 365 nm, beamsplitter at 395 nm, and emission at 445 nm). In some cases, stacks of optical sections were acquired at different step sizes between 0.4 and 0.8 μm . Images were processed and analyzed using the AxioVision software (Rel. 4.8.2) (Zeiss, Jena, Germany). To ensure unbiased acquisition of images, the MosaiX-module sampling system (Zeiss, Jena, Germany) was employed automatically recording individual cells and assembling a large panel of cells covering an area of 5 \times 5 mm consisting of 266 individual images. The individual stages as defined in Figure 1 were scored from those composite images. For the staging (Figure 4), 5,000–7,500 individual cells from 30 independent experimental series were pooled. Stages were defined as follows: *stage 0* round, no cell wall; *stage 1* cell wall present upon staining with Calcofluor White, nucleus central; *stage 2* ovoid shape with a ratio of longer axis to shorter axis of >1.2 (Figure S1B), *stage 3* elongate with a ratio of longer axis to shorter axis of >2.0. For the drug, peptide, and temperature studies (Figure 6–8), typically between 500 and 1,500 individual cells from 2–3 independent experiments were scored. Mortality (Figure S3) was determined from loss of membrane integrity (e.g. loss of shape and rough outline due to cytoplasm leaking out) and breakdown of cytoplasmic structure visible in the differential-interference contrast, with 500–2,000 individual cells scored for a single experiment.

Acknowledgements

This work was supported by funds from the Sino-German Center for Research Promotion, GZ 614 “Probing the Self-Organization

of Plant Cells by Micropattern and Microfluidics". The standardization of the regeneration system was made possible due to the very precise and standard cultivation system provided by Sabine Purper.

Received 22 Aug. 2012 Accepted 15 Oct. 2012

References

- Akashi T, Kawasaki S, Shibaoka H** (1990) Stabilization of cortical microtubules by the cell wall in cultured tobacco cells. Effects of extensin on the cold-stability of cortical microtubules. *Planta* **182**, 363–369.
- Baluška F, Šamaj J, Wojtaszek P, Volkmann D, Menzel D** (2003) Cytoskeleton plasma membrane-cell wall continuum in plants. Emerging links revisited. *Plant Physiol.* **133**, 482–491.
- Bhatla SC, Kießling J, Reski R** (2002) Observation of polarity induction by cytochemical localization of phenylalkylamine-binding receptors in regenerating protoplasts of the moss *Physcomitrella patens*. *Protoplasma* **219**, 99–105.
- Bloch R** (1965) Polarity and gradients in plants. A survey. In: Ruhland W, ed. *Encyclopedia of Plant Physiology*. vol. 15. Springer-Verlag, Heidelberg. pp. 234–274.
- Bode PM, Bode HR** (1984) Patterning in *Hydra*. In: Malacinski GM, Bryant SV, eds. *Pattern Formation*. MacMillan, London New York. pp. 213–241.
- Boveri T** (1901) Über die Polarität des Seeigeeleies. *Verhandlungen der physikalisch-medizinischen Gesellschaft Würzburg* **34**, 145–175.
- Brawley SH, Robinson KR** (1985) Cytochalasin treatment disrupts the endogenous currents associated with cell polarization in fucoid zygotes: Studies of the role of F-actin in embryogenesis. *J. Cell Biol.* **100**, 1173–1184.
- Canut H, Carrasco A, Galaud JP, Cassan C, Bouyssou H, Vita N, Ferrara P, Pont-Lezica R** (1998) High affinity RGD-binding sites at the plasma membrane of *Arabidopsis thaliana* links the cell wall. *Plant J.* **16**, 63–71.
- Dhonukshe P, Kleine-Vehn J, Friml J** (2005) Cell polarity, auxin transport, and cytoskeleton-mediated division planes: Who comes first? *Protoplasma* **226**, 67–73.
- Dhonukshe P, Tanaka H, Goh T, Ebine K, Mähönen AP, Kalika Prasad K, Bliilou I, Geldner N, Xu J, Uemura T, Chory J, Ueda T, Nakano A, Scheres B, Friml J** (2008) Generation of cell polarity in plants links endocytosis, auxin distribution and cell fate decisions. *Nature* **456**, 962–967.
- Edwards ES, Roux SJ** (1994) Limited period of graviresponsiveness in germinating spores of *Ceratopteris richardii*. *Planta* **195**, 150–152.
- Edwards ES, Roux SJ** (1997) The influence of gravity and light on developmental polarity of single cells of *Ceratopteris richardii* gametophytes. *Biol. Bull.* **192**, 139–140.
- Emons AMC, Mulder BM** (1998) The making of the architecture of the plant cell wall: How cells exploit geometry. *Proc. Natl. Acad. Sci. USA* **95**, 7215–7219.
- Frey N, Klotz J, Nick P** (2010) A kinesin with calponin-homology domain is involved in premitotic nuclear migration. *J. Exp. Bot.* **61**, 3423–3437.
- Fujita M, Himmelspach R, Hocart CH, Williamson RE, Mansfield SD, Wasteneys GO** (2011) Cortical microtubules optimize cell-wall crystallinity to drive unidirectional growth in *Arabidopsis*. *Plant J.* **66**, 915–928.
- Geitmann A, Ortega JK** (2009) Mechanics and modeling of plant cell growth. *Trends Plant Sci.* **14**, 467–478.
- Goodner B, Quatrano RS** (1993) *Fucus* embryogenesis: A model to study the establishment of polarity. *Plant Cell* **5**, 1471–1481.
- Green PB** (1962) Mechanism for plant cellular morphogenesis. *Science* **138**, 1404–1405.
- Green PB** (1980) Organogenesis – a biophysical view. *Annu. Rev. Plant Physiol.* **31**, 51–82.
- Hable WE, Hart PE** (2010) Signaling mechanisms in the establishment of plant and fucoid algal polarity. *Mol. Repr. Develop.* **77**, 751–758.
- Haigler CH, Brown RM** (1986) Transport of rosettes from the Golgi apparatus to the plasma membrane in isolated mesophyll cells of *Zinnia elegans* during differentiation to tracheary elements in suspension culture. *Protoplasma* **134**, 111–120.
- Hohenberger P, Eing C, Straessner R, Durst S, Frey W, Nick P** (2011) Plant actin controls membrane permeability. *BBA Membranes* **1808**, 2304–2312.
- Holweg CL** (2007) Living markers for actin block myosin-dependent motility of plant organelles and auxin. *Cell Motil. Cytoskel.* **64**, 69–81.
- Jaffe LF** (1966) Electrical currents through the developing *Fucus* egg. *Proc. Natl. Acad. Sci. USA* **56**, 1102–1109.
- Klotz J, Nick P** (2012) A novel actin-microtubule cross-linking kinesin, NtKCH, functions in cell expansion and division. *New Phytol.* **193**, 576–589.
- Kranz E, Lörz H** (1993) *In vitro* fertilization with isolated, single gametes results in zygotic embryogenesis and fertile maize plants. *Plant Cell* **5**, 739–746.
- Kuss-Wymer CL, Cyr RJ** (1992) Tobacco protoplasts differentiate into elongate cells without net microtubule depolymerization. *Protoplasma* **168**, 64–72.
- Li S, Lei L, Somerville CR, Gua Y** (2012) Cellulose synthase interactive protein 1 (CS1) links microtubules and cellulose synthase complexes. *Proc. Natl. Acad. Sci. USA* **109**, 185–190.
- Lintilhac PM** (1999) Towards a theory of cellularity – speculations on the nature of the living cell. *Bioscience* **49**, 60–68.
- Maeda H, Ishida N** (1967) Specificity of binding of hexopyranosyl polysaccharides with fluorescent brightener. *J. Biochem.* **62**, 276–278.
- Maisch J, Nick P** (2007) Actin is involved in auxin-dependent patterning. *Plant Physiol.* **143**, 1695–1704.
- Murata T, Wada M** (1991) Effects of centrifugation on preprophase-band formation in *Adiantum* protonemata. *Planta* **183**, 391–398.

- Nagata T, Nemoto Y, Hasezawa S** (1992) Tobacco BY-2 cell line as the “HeLa” cell in the cell biology of higher plants. *Int. Rev. Cytol.* **132**, 1–30.
- Nagata T, Takebe I** (1970) Cell wall regeneration and cell division in isolated tobacco mesophyll protoplasts. *Planta* **92**, 301–308.
- Nick P** (2010) Probing the actin-auxin oscillator. *Plant Signal. Behav.* **5**, 4–9.
- Nick P** (2011) Mechanics of the cytoskeleton. In: P. Wojtaszek, ed. *Mechanical Integration of Plant Cells and Plants*. Springer-Verlag, Berlin-Heidelberg. pp. 53–90.
- Nick P, Furuya M** (1992) Induction and fixation of polarity – Early steps in plant morphogenesis. *Dev. Growth Differ.* **34**, 115–125.
- Örvar BJ, Sangwan V, Omann F, Dhindsa RS** (2000) Early steps in cold sensing by plant cells: The role of actin cytoskeleton and membrane fluidity. *Plant J.* **23**, 785–794.
- Paredez AR, Somerville CR, Ehrhardt DW** (2006) Visualization of cellulose synthase demonstrates functional association with microtubules. *Science* **312**, 1491–1495.
- Peera WA, Blakeslee JJ, Yang H, Murphy AS** (2011) Seven things we think we know about auxin transport. *Mol. Plant* **4**, 487–504.
- Pickard BG** (2007) Delivering force and amplifying signals in plant mechanosensing. *Curr. Top. Membr.* **58**, 361–392.
- Pickard BG** (2008) “Second extrinsic organizational mechanism” for orienting cellulose: Modeling a role for the plasmalemmal reticulum. *Protoplasma* **233**, 1–29.
- Preston RD** (1955) Mechanical properties of the plant cell wall. In: W. Ruhland, ed. *Handbuch der Pflanzenphysiologie vol. 1*. Springer-Verlag, Berlin-Göttingen-Heidelberg. pp. 745–751.
- Sano T, Higaki T, Oda Y, Hayashi T, Hasezawa S** (2005) Appearance of actin microfilament ‘twin peaks’ in mitosis and their function in cell plate formation, as visualized in tobacco BY-2 cells expressing GFP-fimbrin. *Plant J.* **44**, 595–605.
- Sijacic L, Liu Z** (2010) Novel insights from live-imaging in shoot meristem development. *J. Integr. Plant Biol.* **52**, 393–399.
- Staiger CJ, Sheahan MB, Khurana P, Wang X, McCurdy DW, Blanchoin L** (2009) Actin filament dynamics are dominated by rapid growth and severing activity in the *Arabidopsis* cortical array. *JCB* **184**, 269–280.
- Smertenko AP, Deeks MJ, Hussey PJ** (2010) Strategies of actin reorganisation in plant cells. *J. Cell Sci.* **123**, 3019–3028.
- Thomas C, Moreau F, Dieterle M, Hoffmann C, Gatti S, Hofmann C, Van Troys M, Ampe C, Steinmetz A** (2007) The LIM Domains of WLIM1 define a new class of actin bundling modules. *J. Biol. Chem.* **282**, 33599–33608.
- Twell D, Park SK, Lalanne E** (1998) Asymmetric division and cell-fate determination in developing pollen. *Trends Plant Sci.* **3**, 305–310.
- Ueda H, Yokota E, Kutsuna N, Shimada T, Tamura K, Shimmen T, Hasezawa S, Dolja VV, Hara-Nishimura I** (2010) Myosin-dependent endoplasmic reticulum motility and F-actin organization in plant cells. *Proc. Natl. Acad. Sci. USA* **107**, 6894–6899.
- Sachs J** (1880) Stoff und Form der Pflanzenorgane. *Arb. Bot. Inst. Würzburg* **2**, 469–479.
- Sun Y, Liu Y, Qu W, Jiang X** (2009) Combining nanosurface chemistry and microfluidics for molecular analysis and cell biology. *Anal. Chim. Acta* **650**, 98–105.
- Vöchting H** (1878) Über Organbildung im Pflanzenreich. Cohen, Bonn.
- Wang YS, Yoo CM, Blancaflor EB** (2008) Improved imaging of actin filaments in transgenic *Arabidopsis* plants expressing a green fluorescent protein fusion to the C and N-termini of the fimbrin actin-binding domain 2. *New Phytol.* **177**, 525–536.
- Williams JG** (1988) The role of diffusible molecules in regulating the cellular differentiation of *Dictyostelium discoideum*. *Development* **103**, 1–16.
- Wyatt SE, Carpita NC** (1993) The plant cytoskeleton – cell wall continuum. *Trends Cell Biol.* **3**, 413–417.
- Wymer C, Wymer SA, Cosgrove DJ, Cyr RJ** (1996) Plant cell growth responds to external forces and the response requires intact microtubules. *Plant Physiol.* **110**, 425–430.

(Co-Editor: Ming Yuan)

Supporting Information

Additional Supporting Information may be found in the online version of this article:

Figure S1. Staging of two individual lines of BY-2 WT.

(A) The cells were originally derived from the Opatrný lab from Prague and the Robinson lab from Heidelberg, respectively. The regeneration shows no significant difference between this independent cell lines.

(B) Definition of *stage 2* by a ratio of longer axis (b) over the shorter axis (a) > 1.2.

Figure S2. Time course for the incidence of individual stages at different temperatures.

Temperatures from 17 °C to 30 °C in non-transformed BY-2 cells (wild-type, WT, white bars), cells expressing GFP in fusion with the actin marker AtFABD2 under control of the cauliflower mosaic virus (CaMV)-35S promoter (AtFABD2, grey bars), and cells expressing GFP in fusion with the microtubule marker AtTuB6 under control of the CaMV-35S promoter (AtTuB6, black bars). Relative frequencies were determined from populations ranging from 1,250 to 3,000 individual cells.

Figure S3. Temperature-sensitivity of the protoplast viability in non-transformed BY-2 cells.

Wild-type (WT, white bars), cells expressing GFP in fusion with the actin marker AtFABD2 under control of the cauliflower mosaic virus (CaMV)-35S promoter (AtFABD2, grey bars), and cells expressing GFP in fusion with the microtubule marker AtTuB6 under control of the CaMV-35S promoter (AtTuB6, black bars). Mortality is shown for day 1 (upper graph) and day 2 (lower graph), i.e., before division of temperature-adapted cells can occur. Mortality was determined from populations of 500 to 2,000 individual cells.